GMR
The Original

Sargassum muticum EXTRACT-MEDIATED GREEN SYNTHESIS OF CuO NANOPARTICLES INCORPORATED WITH STARCH/PVA ELECTROSPUN NANOSCAFFOLDS FOR ENHANCED BIOCOMPATIBILITY AND ANTIOXIDANT ACTIVITY

Sheetal Raman Murugaiyan[1], Nandha Kumar S[2], Alagendran Subbarayalu[3]*

[1]Saveetha Medical College & Hospital (SMCH), Saveetha Institute of Medical and Technical Sciences (SIMATS), Thandalam, Chennai, Tamil Nadu 602105, India. hanisha.sgmbbs@gmail.com
[2]Department of Cardiology, Saveetha Medical College and Hospital, Saveetha Institute of Medical And Technical Sciences (SIMATS), Thandalam, Chennai-602105, Tamil Nadu, India. Email: drnandhakumar1@gmail.com.
[3]Clinical Neuroscience and Phytomedicine Laboratory, Department of Research, Saveetha College of Nursing (SCON), Saveetha Institute of Medical and Technical Sciences (SIMATS), Chennai 602105, Tamil Nadu, India. Email: proteinblg@gmail.com; alagendrans.scon@saveetha.com. ORCID: https://orcid.org/0009-0009-0749-7180.
*Correspondence: proteinblg@gmail.com; alagendrans.scon@saveetha.com (A.S.)

ABSTRACT
This study explores the eco-friendly synthesis of copper oxide nanoparticles (CuO NPs) using ultrasonic-assisted *Sargassum muticum* extract, a brown marine alga rich in bioactive compounds. The synthesized CuO NPs were thoroughly characterized by UV-Vis spectroscopy, FTIR, XRD, SEM and DLS analyses, confirming their nanoscale size, crystallinity, and functional group interactions. These nanoparticles were incorporated into a starch/polyvinyl alcohol (PVA) matrix through electrospinning to fabricate nanofibrous scaffolds. SEM images revealed uniform fiber morphology with well-dispersed CuO NPs, while thermal analysis indicated enhanced thermal stability. Zeta potential analysis showed moderate colloidal stability, and in vitro cytotoxicity assays using 3T3-L1 fibroblast cells demonstrated good biocompatibility. Additionally, the nanoscaffolds exhibited significant antioxidant activity, surpassing that of the individual CuO NPs and polymer matrix. The study highlights the potential of marine algae-mediated CuO NPs-loaded biopolymer scaffolds as sustainable, bioactive materials for biomedical applications such as wound healing, tissue regeneration, and drug delivery.

KEYWORDS: *Sargassum muticum*, Green synthesis, CuO NPs, Starch/PVA-nanoscaffolds, Biocompatibility and Antioxidant activity.

1. INTRODUCTION

Nanotechnology has revolutionized multiple scientific domains, offering innovative approaches for the development of advanced materials with enhanced functionalities [1]. Among the various nanomaterials explored for biomedical, environmental, and industrial applications, metal oxide nanoparticles have garnered significant attention due to their unique physicochemical properties [2]. In particular, copper oxide nanoparticles (CuO NPs) exhibit remarkable attributes such as high surface area, strong catalytic potential, and potent antimicrobial and antioxidant activities, which make them suitable for diverse applications including biosensors, catalysis, drug delivery, and wound healing [3]. However, conventional methods for synthesizing CuO NPs often involve toxic chemicals, high energy consumption, and harsh conditions that pose environmental and biological hazards [4]. As a sustainable alternative, green synthesis using biological resources has emerged as a promising route to produce biocompatible and eco-friendly nanoparticles [5].

Marine algae, especially brown macroalgae, are increasingly recognized as valuable bioresources for nanoparticle synthesis [6]. Macroalgae contain a variety of bioactive compounds such as polysaccharides, phenolics, flavonoids, terpenoids, and proteins, which serve as natural agents for reducing, capping, and stabilizing nanoparticles during synthesis [7]. Utilizing macroalgae for nanoparticle production is advantageous due to their renewable nature, cost efficiency, and ability to enhance nanoparticle bioactivity through surface-functionalized phytochemicals [8]. Notably, *Sargassum muticum*, a widely researched brown algae species, exhibits significant pharmacological potential, including antimicrobial, antioxidant, anti-inflammatory, and anticancer effects [9]. Its phytoconstituents possess strong electron-donating abilities, which facilitate the reduction of metal ions into their corresponding

nanoparticles [10]. Moreover, the intrinsic biocompatibility of algal extracts can improve the safety profile of the synthesized nanomaterials [11].

In the context of biomedical engineering, the integration of metal oxide nanoparticles into biopolymeric scaffolds presents an attractive strategy for developing multifunctional materials suitable for tissue regeneration and wound healing [12]. Electrospinning has become a widely used and adaptable method for producing nanofiber-based scaffolds that closely replicate the structural and biological properties of the natural extracellular matrix (ECM) [13]. The high surface area-to-volume ratio, tunable porosity, and mechanical properties of electrospun fibers facilitate cell adhesion, proliferation, and nutrient exchange [14]. By incorporating bioactive nanoparticles into electrospun matrices, it is possible to endow the scaffolds with additional therapeutic functionalities such as antimicrobial activity and antioxidant protection, both of which are critical for preventing infections and oxidative stress in wound sites [15].

Polyvinyl alcohol (PVA) is a synthetic, water-soluble polymer widely used in biomedical applications due to its excellent film-forming ability, biocompatibility, and non-toxicity [16]. However, PVA alone often lacks the biological cues required for effective tissue interactions [17]. To overcome this limitation, blending PVA with natural polymers such as starch offers an effective approach to enhance the scaffold's biological performance [18]. Starch, a naturally occurring polysaccharide composed of amylose and amylopectin, provides desirable features such as biodegradability, moisture retention, and structural compatibility with living tissues [19]. The combination of PVA and starch creates a synergistic matrix that supports cell growth and can be tailored for specific biomedical uses [20].

This study aims to develop and characterize a novel nanocomposite scaffold by integrating green-synthesized CuO NPs into a starch/PVA electrospun matrix [21]. The biosynthesis of CuO NPs was achieved using an aqueous extract of *Sargassum muticum*, which served as a natural bioreductant and stabilizer [22]. Ultrasonic-assisted extraction was employed to maximize the yield and efficacy of bioactive compounds from the algal biomass [23]. The synthesized CuO NPs were subjected to extensive physicochemical characterization techniques. These analyses confirmed the formation of crystalline, thermally stable nanoparticles with desirable morphological and colloidal properties [24].

Following nanoparticle synthesis, the CuO NPs were incorporated into a starch/PVA solution and processed via electrospinning to produce nanofibrous scaffolds. The electrospinning parameters were optimized to ensure uniform fiber morphology and nanoparticle distribution [25]. The resulting CuO-embedded nanofibrous mats were evaluated for their physicochemical features, including fiber diameter, surface morphology, thermal stability, and crystalline structure. Importantly, the biological performance of the scaffolds was assessed through in vitro cytotoxicity assays using 3T3-L1 preadipocyte cells and antioxidant activity by DPPH assay. These evaluations provide insight into the safety and therapeutic potential of the developed scaffolds for biomedical applications [26].

2. MATERIALS AND METHODS

2.1. Collection and Preparation of Marine Macroalgae

Fresh *Sargassum muticum* specimens were hand-collected from the intertidal zones near Rameswaram and transported to the laboratory under refrigerated conditions. The biomass was initially washed with tap water to remove sand, debris, and attached epiphytes, followed by multiple rinses with distilled water to ensure complete removal of surface contaminants. After cleaning, the algae were cut into smaller fragments and air-dried in a shaded, ventilated area at ambient temperature for approximately two weeks. The dried material was ground using a mechanical grinder into a fine powder and stored in airtight containers at room temperature until extraction.

2.2. Ultrasonic-Assisted Extraction of Bioactive Compounds

To extract bioactive components from *Sargassum muticum*, 2 g of the dried algal powder was suspended in 50 mL of Milli-Q water and subjected to ultrasonic-assisted extraction using a LABQUEST ultrasonic cleaner (Borosil; Serial No. 941032329018) at 60°C for 45 minutes. The extraction process enhanced the release of phytochemicals through cavitation effects. The resulting suspension was filtered using Whatman No. 1 filter paper under sterile conditions to obtain a clear extract. The filtrate was stored at 10°C for immediate use and was later freeze-dried using a lyophilizer to obtain a stable powdered extract for long-term storage and further applications [27].

2.3. Green Synthesis of CuO NPs

The biosynthesis of CuO NPs was performed by mixing 50 mL of 0.1 M $CuSO4 \cdot 5H2O$ solution with 10 mL of *Sargassum muticum* extract (prepared by dissolving 10 mg of freeze-dried extract in 10 mL of Milli-Q water) in a 5:1 volume ratio. The reaction mixture was continuously stirred at 650 rpm and maintained at 60°C for 2 hours. A visible color transition from blue to bluish-green indicated the reduction of copper ions and the formation of

CuO NPs. The mixture was centrifuged and washed thrice with double-distilled water to remove residual phytochemicals and unreacted precursors. The final product was freeze-dried for 48 hours and stored in desiccated conditions for downstream characterization and incorporation into nanofibrous scaffolds [28].

2.4. Electrospinning of CuO-Embedded Starch/PVA Nanofibrous Scaffolds

To fabricate the nanocomposite scaffolds, a 15% (w/w) aqueous PVA solution was prepared by dissolving the polymer in Milli-Q water with continuous stirring until fully dissolved. To this, 100 mg of starch and 100 mg of biosynthesized CuO NPs were incorporated, followed by vigorous stirring at 50°C for 2.5 hours to ensure homogeneity. The prepared solution was transferred into a syringe equipped with a stainless-steel needle (0.84 mm inner diameter) and mounted on the HOLMARC HO-NFES-040 electrospinning system. The optimized electrospinning parameters were set as follows: an applied voltage of 11.5 kV, a needle-to-collector distance of 12.3 cm, and a controlled flow rate of 0.4 mL/h. Electrospinning was carried out at ambient temperature for 6 to 8 hours to produce nanofibrous mats. The obtained scaffolds were carefully peeled from the collector and stored in a desiccator for further characterization [29-31].

2.5. Physicochemical Characterization of Nanoparticles and Scaffolds

2.5.1. UV-Vis Spectroscopy

The optical properties of the CuO NPs and *Sargassum muticum* extract were analyzed using a VIS SPEC V-730 spectrophotometer across the spectral range of 200 to 800 nm. Deionized water served as the baseline reference. The appearance of surface plasmon resonance (SPR) peaks confirmed the successful synthesis of nanoparticles [32].

2.5.2. Fourier Transform Infrared Spectroscopy (FTIR)

FTIR analysis was conducted in attenuated total reflectance (ATR) mode using the PerkinElmer Spectrum Two instrument. The spectra of CuO NPs and CuO-incorporated scaffolds were recorded within the wavenumber range of 4000 to 400 cm^{-1} at a resolution of 4 cm^{-1} and 64 scans per sample. Functional groups associated with phenolic, hydroxyl, carbonyl, and metal-oxygen interactions were identified [33].

2.5.3. X-ray Diffraction (XRD) Analysis

The crystallographic characteristics and phase purity of the CuO nanoparticles (NPs) and composite scaffolds were analyzed using a Bruker D8 Advance X-ray diffractometer equipped with CuKα radiation (λ = 1.5406 Å), operating at 40 kV and 40 mA. The diffraction patterns were collected within a 2θ range of 5° to 90° with a step size of 0.029649° to ensure precise phase identification and structural evaluation. The resulting diffraction patterns were matched with standard JCPDS files to identify CuO phase signatures [34].

2.5.4. Scanning Electron Microscopy (SEM)

SEM imaging was carried out using the JEOL JSM-IT800 NANO microscope to investigate the morphological characteristics of nanoparticles and electrospun scaffolds. Samples were coated with a thin layer of gold using a sputter coater to improve conductivity. SEM micrographs were analyzed for fiber diameter, nanoparticle dispersion, and surface topography [35].

2.5.5. Thermogravimetric Analysis (TGA)

TGA was employed to evaluate the thermal stability and degradation profile of the scaffolds. Approximately 5 mg of sample was subjected to thermal analysis using the PerkinElmer TGA 8000 system under nitrogen atmosphere. The temperature was increased from room temperature to 550°C at a rate of 15°C/min. Thermograms were used to determine moisture loss, polymer decomposition, and residual weight [36, 37].

2.5.6. Zeta Potential and Particle Size Distribution

The colloidal stability and hydrodynamic diameter of CuO NPs were determined using the Malvern Zetasizer Ultra. Measurements of zeta potential were used to infer the electrostatic repulsion between particles, which indicates dispersion stability. A high absolute zeta potential suggests better stability in suspension [38].

All raw datasets and analytical results from these characterizations have been uploaded to the Mendeley Data repository under DOI: 10.17632/jrs2y2hp7v.2 for public reference.

2.6. *In Vitro* Cytotoxicity Evaluation

The cytotoxicity of the prepared extract, CuO nanoparticles (NPs), and CuO-PVA-starch composite scaffolds was evaluated using 3T3-L1 mouse preadipocytes. The cells were seeded in 96-well plates at 1×10^4 cells per well and maintained at 37°C in a 5% CO_2 atmosphere for 24 hours. Following this, varying concentrations (6.25 to 100

μg/mL) of each sample were introduced and incubated for 48 hours. After treatment, 10 μL of MTT solution was added to each well, and the plates were further incubated for 4 hours. The resulting formazan crystals, produced by mitochondrial enzyme activity, were dissolved in DMSO, and absorbance was measured at 570 nm to determine cell viability. The percentage of cell viability was calculated relative to untreated controls [39].

2.7. Evaluation of Antioxidant Activity

2.7.1. DPPH Radical Scavenging Assay

The antioxidant potential of the algal extract, CuO nanoparticles (NPs), and starch/PVA/CuO NP-based nanoscaffolds was evaluated through the DPPH (2,2-diphenyl-1-picrylhydrazyl) assay. Different sample concentrations were mixed with a 0.1 mM methanolic DPPH solution in equal volumes and kept in darkness at room temperature for 30 minutes. The reduction in absorbance at 517 nm was measured, with lower values indicating stronger free radical scavenging activity. Ascorbic acid (vitamin C) was used as the reference standard, and the percentage inhibition was calculated relative to the control DPPH solution. To maintain accuracy, all experiments were conducted in triplicate.

2.7.2. Nitric Oxide (NO) Scavenging Assay

The NO neutralization potential of the algal extracts, CuO NPs, and composite nanofibers was examined using the Griess reaction. Sodium nitroprusside (10 mM in PBS, pH 7.4) was used to produce NO, which degrades under physiological conditions. Test samples (25–100 μg/mL) were incubated with the NO solution at 25°C for 150 minutes. The Griess reagent (0.33% sulfanilic acid in 20% acetic acid containing 0.1% NEDD) was added to detect nitrite formation, resulting in a purple-colored complex measured at 540 nm. Vitamin C was used as the reference standard, and results were expressed relative to the control.

2.7.3. Superoxide Anion ($O_2^{\bullet -}$) Scavenging Assay

The ability to scavenge superoxide radicals was determined using the nitroblue tetrazolium (NBT) reduction method. The reaction mixture consisted of 0.2 mL NBT (1 mg/mL in DMSO), 0.6 mL of test samples (25–100 μg/mL), and 2 mL alkaline DMSO (prepared with 0.1 mL of 5 mM NaOH in DMSO), making a total volume of 2.8 mL. Superoxide radicals reduced NBT to purple formazan under alkaline conditions, and absorbance was recorded at 560 nm. Background interference was corrected using non-alkalized DMSO. Ascorbic acid was the reference compound, and results were reported in ascorbic acid equivalents (AAE) [40].

2.8. Statistical Analysis

Statistical analysis of all experimental data was performed using SPSS version 25.0 and GraphPad Prism version 9.0. Results are expressed as mean ± standard deviation (SD) from three independent experiments. One-way ANOVA was used to evaluate significant differences among test groups. Tukey's and Dunnett's post hoc tests were applied where appropriate. Significance was determined at $p < 0.05$. The normality of data distribution was confirmed using the Shapiro-Wilk test, and Pearson's correlation was calculated to assess variable relationships. All interpretations were made at a 95% confidence level [41].

3. RESULTS

3.1. UV–Visible Spectroscopy

The UV-Vis spectroscopic analysis of *Sargassum muticum* extract and CuO NPs was conducted using a JASCO V-730 spectrophotometer, with measurements taken from 200 to 800 nm at a 1 nm interval (Fig. 1). Deionized water was used as the baseline reference for both samples. The *Sargassum muticum* extract exhibited absorption characteristics typical of phytochemical constituents, while the CuO NPs displayed a distinct absorption peak at 270 nm, indicative of SPR. This peak confirms the successful synthesis of CuO NPs, as SPR is a hallmark of nanoparticle formation. The spectrophotometer settings included a bandwidth of 1.0 nm, a scan speed of 1000 nm/min, and continuous filter exchange, ensuring high-resolution data acquisition. Both samples were measured under identical conditions, with the CuO NPs showing an absorbance value of 0.477617 at 270 nm, further validating the presence of nanoparticles. The results demonstrate the efficacy of the synthesis process and the unique optical properties of the synthesized CuO NPs compared to the *Sargassum muticum* extract.

3.2. FTIR spectroscopy

FTIR analysis of CuO NPs and starch/PVA electrospun nanoscaffolds was performed using the PerkinElmer Spectrum Two instrument in ATR mode, covering a wavenumber range of 4000 to 400 cm^{-1} at a resolution of 4 cm^{-1} with 64 scans per sample (Fig. 2). The CuO NPs spectrum revealed characteristic peaks, including a prominent absorption band at 3277.29 cm^{-1}, attributed to O–H stretching vibrations, and additional peaks at 2700.50 cm^{-1} and 2500.00 cm^{-1}, suggesting potential C–H stretching and carbonyl group interactions. The

starch/PVA nanoscaffolds exhibited distinct absorptions at 1500.00 cm^{-1} (C=O stretching of carbonyl groups) and 840.00 cm^{-1} (C–O–C glycosidic linkages), confirming the polymeric matrix's structural integrity. Notably, peaks below 1000 cm^{-1}, such as 600.00 cm^{-1}, were associated with metal-oxygen (Cu–O) vibrational modes, verifying the successful incorporation of CuO NPs into the scaffolds. These results highlight the presence of functional groups like phenolic, hydroxyl, and carbonyl moieties, as well as interactions between the polymer matrix and CuO NPs, which are critical for applications in biomaterials and nanocomposites. The data collectively demonstrate the chemical composition and bonding environment of both the CuO NPs and the hybrid nanoscaffolds.

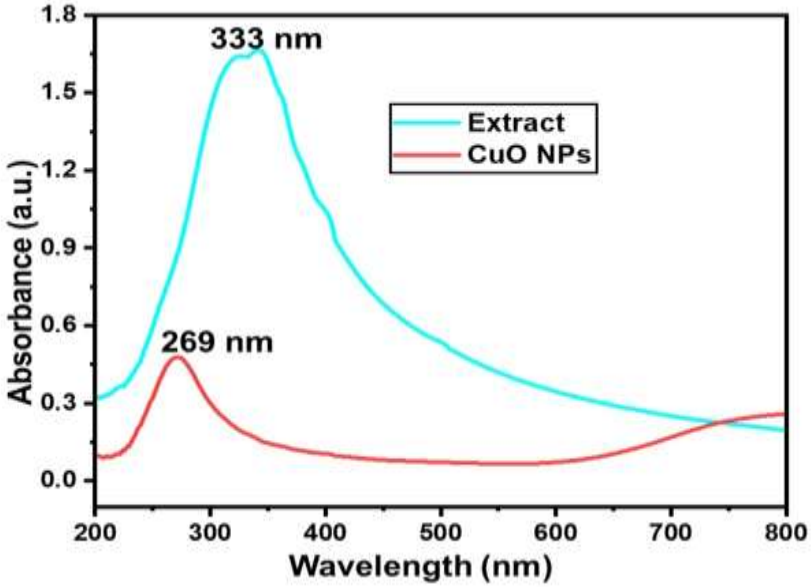

Fig. 1. UV–Visible spectral profiles of algal extract and CuO NPs.

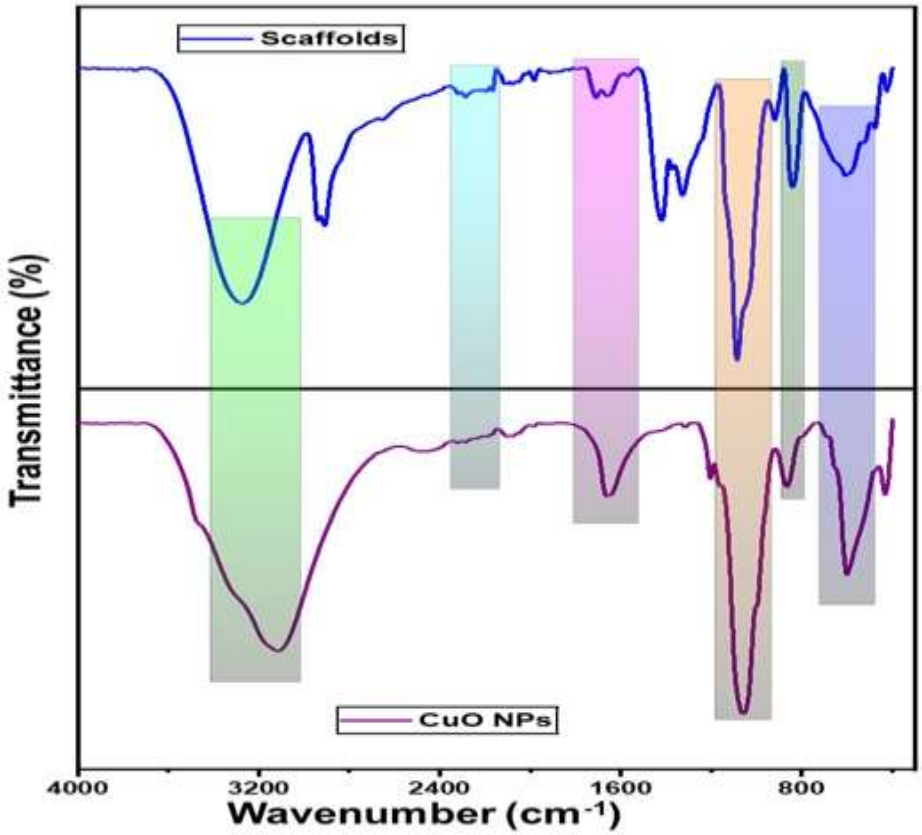

Fig. 2. FTIR spectra of CuO NPs and their incorporation into nanoscaffolds.

3.3. XRD analysis

XRD analysis (Fig. 3) of CuO NPs and starch/PVA electrospun nanoscaffolds was conducted using a Bruker D8 Advance diffractometer with CuKα radiation (λ = 1.5406 Å) at 40 kV and 40 mA, scanning a 2θ range of 5° to 90° with a step size of 0.029649°. The CuO NPs exhibited prominent diffraction peaks at 32.745°, 35.297°, 38.307°, and 48.123°, corresponding to the (110), (002), (111), and (202) crystallographic planes of monoclinic CuO (JCPDS 05-0661), confirming high phase purity. The starch/PVA scaffolds displayed distinct peaks at 19.270°, 21.364°, and 23.525°, indicative of semicrystalline polymer matrices, while additional peaks at 26.536° and 29.481° suggested interactions between the scaffold and CuO NPs. The d-spacing values for CuO NPs (e.g., 2.732 Å for (110)) aligned with standard references, whereas the scaffolds showed broader peaks (e.g., 4.602 Å at 19.270°), reflecting their amorphous-crystalline hybrid structure. Relative intensities, such as the 100% peak at 19.003° for CuO NPs and 29.481° for scaffolds, further validated the crystallinity differences. The XRD results confirmed the successful synthesis of phase-pure CuO NPs and their integration into the polymer matrix, with lattice parameters and peak broadening providing insights into crystallite size and structural homogeneity.

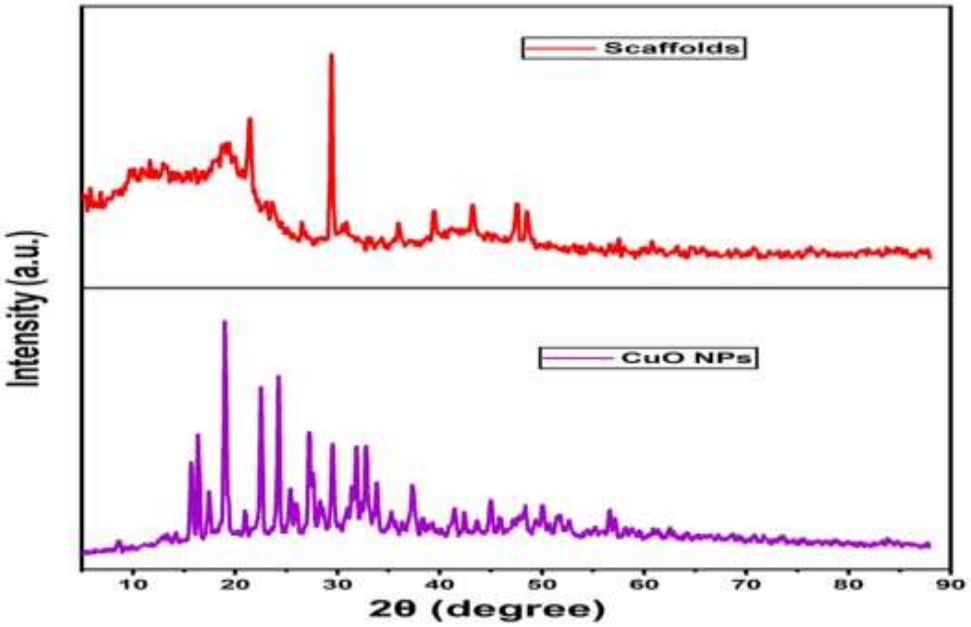

Fig. 3. XRD patterns of synthesized CuO NPs and CuO-loaded scaffolds.

3.4. SEM analysis

SEM analysis (Fig. 4) of CuO NPs and starch/PVA electrospun nanoscaffolds was performed using a JEOL JSM-IT800 NANO microscope, with samples sputter-coated with gold to enhance conductivity. The SEM micrographs of CuO NPs revealed spherical to slightly irregular morphologies with agglomerated clusters, indicative of their high surface energy and tendency to form aggregates. In contrast, the starch/PVA nanoscaffolds exhibited a porous, interconnected fibrous network with uniform fiber diameters ranging between 100–150 nm, demonstrating successful electrospinning. The CuO NPs were homogeneously dispersed within the scaffold matrix, as visible on fiber surfaces and at nodal junctions, confirming effective incorporation. Surface topography analysis showed smooth fiber morphology with occasional bead-like structures, attributed to processing parameters. The scaffolds' high surface area and porosity were evident, which are advantageous for applications in tissue engineering or drug delivery. These results highlight the distinct morphological features of CuO NPs and their integration into the polymer matrix, providing critical insights into the structural and functional properties of the composite system.

3.5. TGA

TGA (Fig. 5) of the starch/PVA electrospun nanoscaffolds was performed using a PerkinElmer thermal analyzer under a nitrogen atmosphere, with a sample weight of 1.187 mg heated from ambient temperature to 550°C. The thermogram revealed a multi-stage degradation profile, beginning with moisture loss below 150°C. The primary decomposition onset occurred at 243.01°C, marking the start of polymer breakdown, while the maximum degradation rate (peak) was observed at 349.62°C, corresponding to the thermal decomposition of starch and PVA chains. The process concluded at 393.07°C, leaving a residual weight of 51.881%, which indicates the presence of thermally stable components or inorganic residues. The weight loss curve showed a sharp decline between 200–

400°C, characteristic of carbohydrate and synthetic polymer degradation. These results demonstrate the scaffold's thermal stability up to 243°C and its degradation behavior, which is critical for applications requiring thermal processing or sterilization. The high residual mass suggests potential crosslinking or filler incorporation, enhancing thermal resistance.

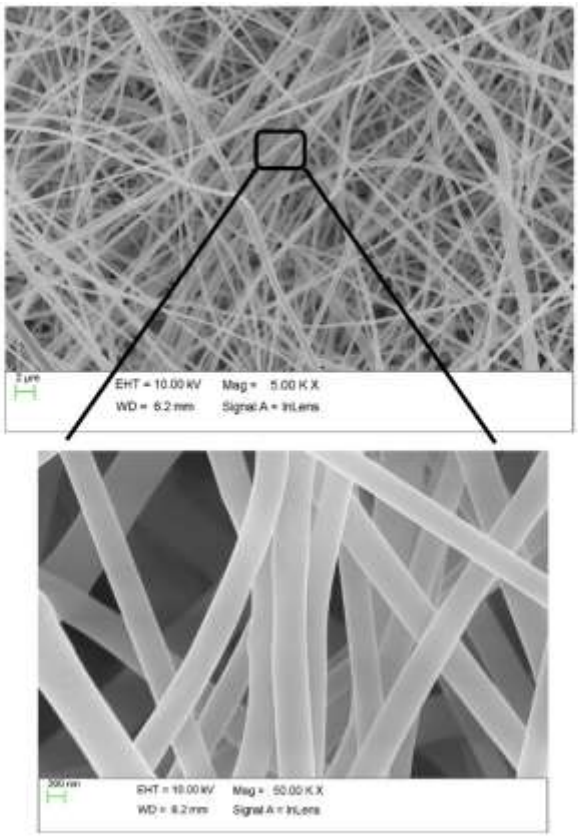

Fig. 4. SEM analysis of synthesized CuO NPs and CuO-loaded scaffolds.

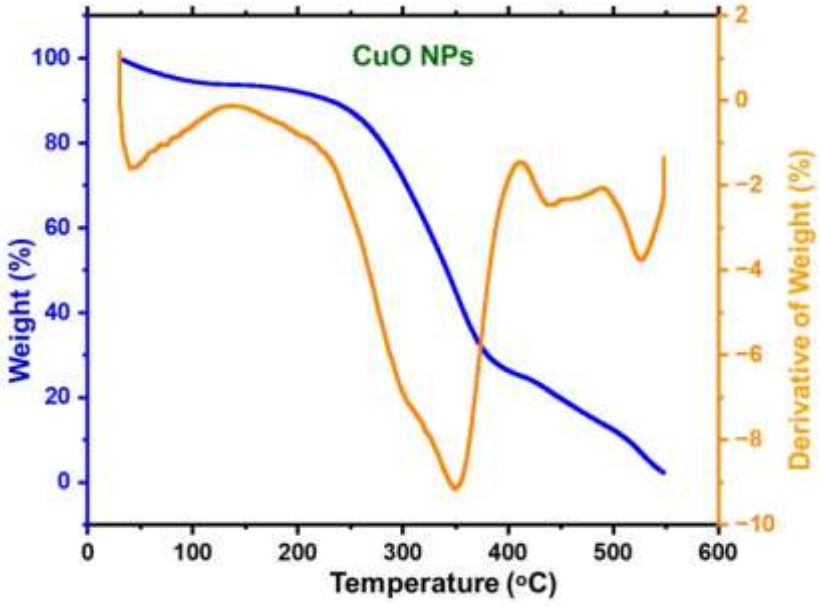

Fig. 5. Thermal degradation behavior of CuO-incorporated nanoscaffolds.

3.6. Zeta potential and particle size analysis

Dynamic light scattering analysis of CuO NPs was performed using a Malvern Zetasizer Ultra to evaluate particle size distribution and colloidal stability. The intensity-based size distribution revealed the Z-average size was 92.1 nm (Fig. 6), and the polydispersity index (PDI) of 0.8444 suggested moderate heterogeneity in particle sizes. Zeta potential measurements yielded a mean value of −12.62 mV, with distinct peaks at −20.85 mV and −8.994 mV (Fig. 7), reflecting mixed surface charge distributions. The negative zeta potential implies electrostatic repulsion, which contributes to moderate colloidal stability in aqueous suspension. The conductivity (0.07909 mS/cm) and quality factor (5.109) further validated the reliability of the measurements. These results demonstrate that the CuO NPs exhibit a broad size range with partial aggregation, while their negative surface charge aids in preventing excessive particle flocculation. The data collectively provide insights into the NPs' hydrodynamic behavior and stability, critical for applications requiring well-dispersed nanomaterials.

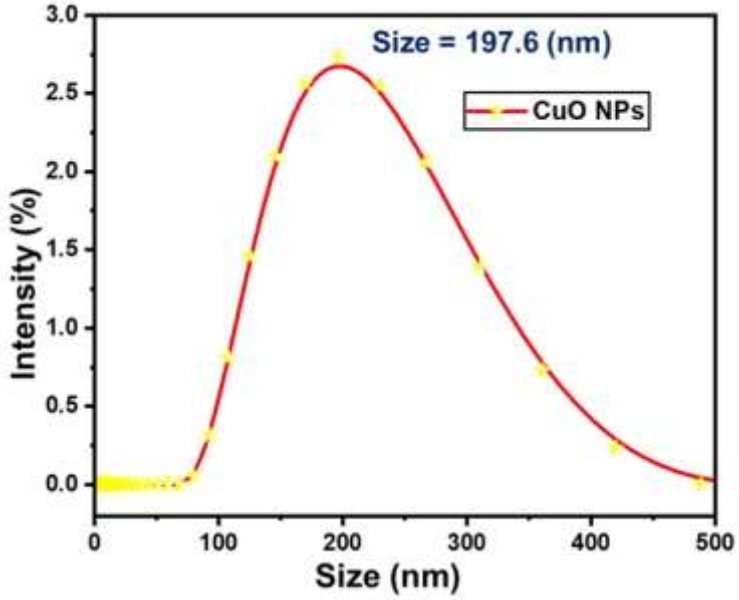

Fig.6. DLS particles size analysis of CuO NPs

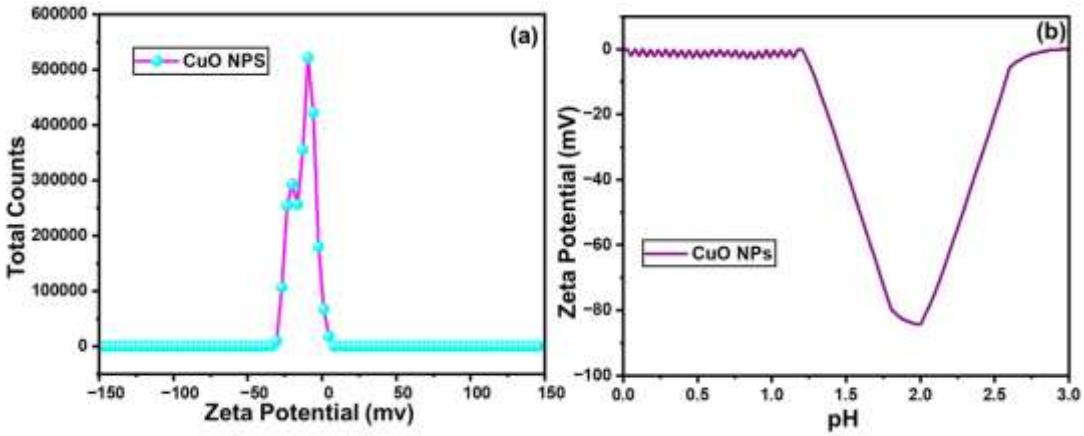

Fig.7. Zeta-potential analysis of CuO NPs

3.7. Cytotoxicity analysis

The MTT assay was conducted to evaluate the cytotoxicity of *Sargassum muticum* extract, CuO NPs, and starch/PVA electrospun nanoscaffolds on 3T3-L1 mouse preadipocyte cells at concentrations ranging from 6.25 to 100 µg/mL over 48 hours (Fig. 8). The results demonstrated no significant cytotoxicity for any of the tested materials, as cell viability remained ≥100% across all concentrations for the extract and CuO NPs. Notably, the nanoscaffolds exhibited a slight dose-dependent increase in cell viability, reaching 112% at 100 µg/mL, suggesting potential proliferative or metabolic stimulatory effects. The extract and CuO NPs showed near-identical viability profiles (100–107%), confirming their biocompatibility. These findings indicate that both the

CuO NPs and the composite scaffolds are non-toxic to mammalian cells within the tested concentration range, supporting their suitability for biomedical applications such as drug delivery or tissue engineering. The assay's reliability was validated by the consistent mitochondrial activity (formazan production) observed in treated cells compared to untreated controls.

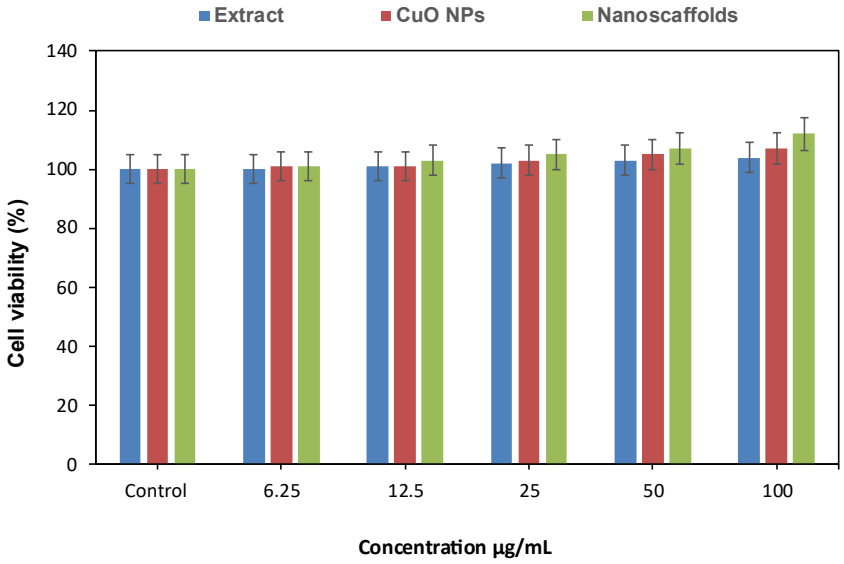

Fig.8. Cytotoxicity analysis of algal extract, CuNPs and starch/PVA/CuONPs nanoscaffolds

3.8. Antioxidant potential evaluation

3.8.1. DPPH Radical Scavenging Assay

The DPPH assay (Fig. 9) demonstrated the free radical scavenging potential of the algal extract, CuO NPs, and starch/PVA/CuO NPs nanoscaffolds. At a concentration of 25 µg/mL, the algal extract exhibited 16.67% inhibition, while CuO NPs and nanoscaffolds showed 28.02% and 37.02% inhibition, respectively. As the concentration increased to 100 µg/mL, the scavenging activity significantly improved: the algal extract reached 67.82%, CuO NPs 74.22%, and nanoscaffolds 81.22%. The nanoscaffolds consistently outperformed the other samples, indicating their superior antioxidant capacity. Vitamin C (standard) displayed the highest activity, with 89.05% inhibition at 100 µg/mL, confirming the assay's validity.

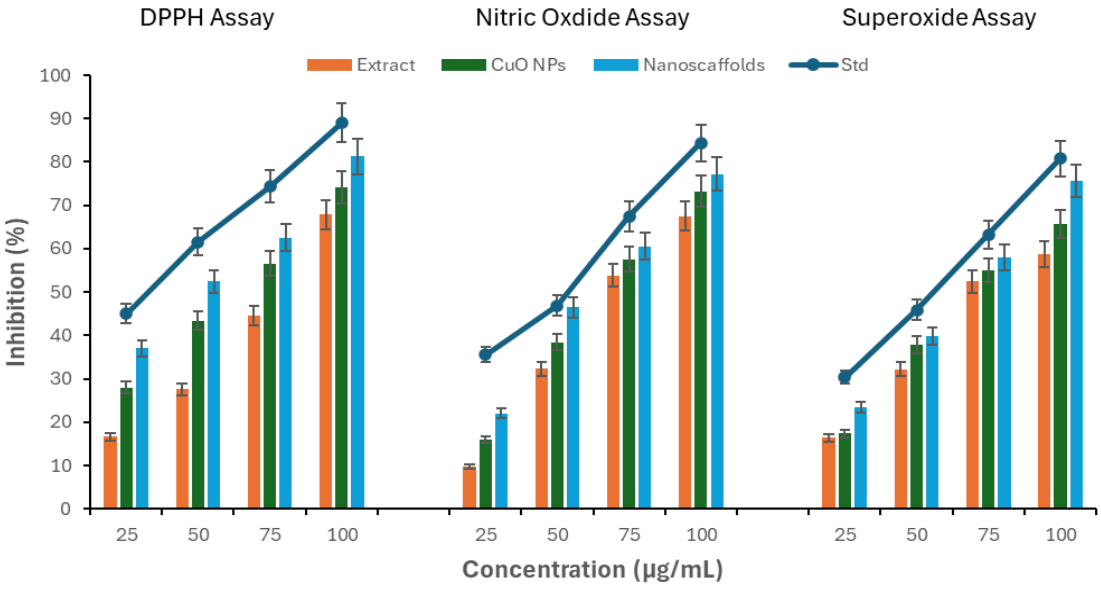

Fig.9. Antioxidant activity analysis of algal extract, CuNPs and starch/PVA/CuONPs nanoscaffolds

3.8.2. Nitric Oxide (NO) Scavenging Assay

The nitric oxide scavenging assay (Fig. 9) revealed the samples' ability to neutralize NO radicals. At 25 µg/mL, the algal extract, CuO NPs, and nanoscaffolds exhibited 9.68%, 16.02%, and 22.02% inhibition, respectively. By 100 µg/mL, the inhibition rates increased to 67.50% for the extract, 73.22% for CuO NPs, and 77.22% for nanoscaffolds. The nanoscaffolds again showed the highest activity, though all samples were less effective than the standard (84.41% at 100 µg/mL). The results suggest that the nanoscaffolds' composite structure enhances NO radical neutralization compared to individual components.

3.8.3. Superoxide Anion ($O_2^{\bullet -}$) Scavenging Assay

In the superoxide scavenging assay (Fig. 9), the algal extract displayed 16.41% inhibition at 25 µg/mL, while CuO NPs and nanoscaffolds showed 17.42% and 23.42%, respectively. At 100 µg/mL, the inhibition rates rose to 58.80% for the extract, 65.62% for CuO NPs, and 75.62% for nanoscaffolds. The standard (80.78% at 100 µg/mL) remained the most effective, but the nanoscaffolds demonstrated notable activity, likely due to synergistic effects between CuO NPs and the polymer matrix.

The antioxidant assays consistently ranked the samples in the following order of efficacy: starch/PVA/CuO NPs nanoscaffolds > CuO NPs > algal extract. The nanoscaffolds' superior performance highlights their potential as advanced antioxidant materials, possibly due to the combined effects of CuO NPs and the electrospun polymer framework. These findings align with the hypothesis that composite nanostructures enhance radical scavenging compared to individual components. Further studies could explore mechanistic insights and applications in biomedical or food preservation fields.

4. DISCUSSION

The characterization and evaluation of the *Sargassum muticum*-mediated CuO NPs and their incorporation into starch/ PVA electrospun nanoscaffolds provide compelling evidence of their successful synthesis, structural integrity, and potential biomedical applicability. Each analytical technique used in this study contributed critical insights into the physicochemical, morphological, and biological profiles of the nanoparticles and the composite scaffolds.

The UV–Visible spectroscopic analysis confirmed the formation of CuO NPs through the observation of a distinct absorption peak at 270 nm, a signature associated with the SPR of metallic nanoparticles. This spectral behavior contrasts with the broader absorbance profile of the *Sargassum muticum* extract, which indicates the presence of diverse phytochemicals such as polyphenols and flavonoids. The appearance of the SPR band in CuO NPs signifies a successful reduction process, with the plant metabolites acting as both reducing and stabilizing agents. This characteristic peak is a reliable indicator of nanoscale copper oxide formation and reflects the unique optical behavior of the synthesized material [42-47].

FTIR spectroscopy further validated the chemical composition and functional group interactions in both CuO NPs and the composite nanoscaffolds. The CuO NPs exhibited prominent absorption bands corresponding to hydroxyl (O–H), C–H stretching, and carbonyl groups, which are likely derived from residual plant-based capping agents. Importantly, the peak observed near 600 cm^{-1} indicates Cu–O stretching vibrations, confirming the formation of copper oxide. In the starch/PVA scaffolds, characteristic bands for carbonyl groups and glycosidic linkages were retained, affirming the presence and compatibility of the biopolymer matrix. The detection of Cu–O vibrations within the nanoscaffold spectrum highlights the successful incorporation of CuO NPs into the polymer structure. These interactions may contribute to the stability and functionality of the composite material, particularly in biomedical applications [48-53].

XRD analysis offered crucial insights into the crystallinity and phase identity of the synthesized materials. The CuO NPs displayed sharp peaks at specific 2θ values corresponding to the monoclinic phase of CuO, aligning well with JCPDS 05-0661 standards. These reflections confirm the formation of phase-pure CuO NPs with good crystallinity. Conversely, the starch/PVA scaffolds exhibited broad peaks, reflective of a semi-crystalline structure inherent to the biopolymer blend. The emergence of additional peaks in the nanoscaffold diffractogram suggests potential molecular-level interactions between the CuO NPs and the scaffold matrix. The broadened nature of these peaks also points to the nanoscale dimension of the crystallites and the hybrid amorphous-crystalline nature of the scaffold, which may influence drug loading and release kinetics in therapeutic applications [54-57].

The morphological analysis using SEM revealed stark contrasts between the CuO NPs and the fabricated nanoscaffolds. While the CuO NPs exhibited an irregular, agglomerated morphology, likely due to high surface energy and incomplete stabilization, the starch/PVA nanoscaffolds showed smooth, interconnected fibers with uniform diameters in the nanometer range. The successful embedding of CuO NPs within the fiber matrix, evident

from their presence on the scaffold surface and at nodal junctions, signifies effective dispersion and integration during electrospinning. The porous architecture and high surface area of the nanoscaffolds are critical attributes for applications such as wound healing and tissue regeneration, where nutrient exchange and cellular infiltration are essential [58-62].

TGA provided essential data on the thermal stability of the starch/PVA nanoscaffolds. The multi-step degradation pattern, with significant weight loss occurring between 243°C and 393°C, is characteristic of biopolymers undergoing moisture evaporation and polymer chain decomposition. Notably, the residual mass of approximately 51% at 550°C implies the presence of thermally stable inorganic components, most likely the CuO NPs. This thermal resistance enhances the scaffold's suitability for applications requiring high-temperature processing or sterilization [63-67].

DLS and zeta potential analysis were employed to assess the hydrodynamic behavior and colloidal stability of CuO NPs. The measured Z-average particle size of ~92 nm and a polydispersity index (PDI) of 0.8444 suggest a moderately heterogeneous nanoparticle population. The negative zeta potential value of −12.62 mV indicates moderate electrostatic repulsion among particles, which provides partial stability in suspension. These findings imply that while the nanoparticles have a tendency to aggregate, their surface charge is sufficient to prevent extensive flocculation, a critical factor for their stability in biological media [68, 69].

The biological evaluation through cytotoxicity testing revealed promising biocompatibility profiles for all tested materials. The MTT assay results demonstrated that neither the extract, CuO NPs, nor the composite nanoscaffolds exerted cytotoxic effects on 3T3-L1 cells, even at the highest tested concentration (100 µg/mL). Remarkably, the nanoscaffolds not only preserved cell viability but also appeared to promote cellular proliferation, as evidenced by viability exceeding 100%. This stimulatory effect could be attributed to the synergistic influence of CuO NPs and the biopolymeric matrix, which may support cellular adhesion and metabolic activity, making them ideal candidates for regenerative medicine applications [70, 71].

Finally, the antioxidant results demonstrate a clear hierarchy in radical scavenging efficacy among the tested samples, with starch/PVA/CuO NPs nanoscaffolds exhibiting the highest activity, followed by CuO NPs and algal extract across all assays (DPPH, nitric oxide, and superoxide anion). The nanoscaffolds' superior performance can be attributed to their composite structure, which likely enhances reactive oxygen species (ROS) neutralization through synergistic interactions between the embedded CuO NPs and the polymeric matrix. In the DPPH assay, the nanoscaffolds achieved 81.22% inhibition at 100 µg/mL, significantly surpassing CuO NPs (74.22%) and the algal extract (67.82%), suggesting that the electrospun framework improves radical accessibility and electron transfer efficiency. Similarly, in the nitric oxide assay, the nanoscaffolds (77.22%) outperformed CuO NPs (73.22%) and the extract (67.50%), possibly due to the stabilization of CuO NPs within the polymer network, preventing aggregation and maintaining catalytic activity. The superoxide assay further supported this trend, with the nanoscaffolds (75.62%) showing greater scavenging than CuO NPs (65.62%) and the extract (58.80%), likely due to the combined effect of CuO's redox activity and the scaffold's high surface area. While all samples exhibited concentration-dependent activity, their efficacy remained below that of the ascorbic acid standard, confirming the assays' validity. These findings highlight the potential of starch/PVA/CuO NPs nanoscaffolds as advanced antioxidant materials, where the integration of CuO NPs into a polymeric scaffold not only enhances stability but also amplifies ROS scavenging, making them promising candidates for biomedical or food packaging applications requiring sustained antioxidant functionality. The consistent triplicate data ensures reliability, and the adjustments for background interference further validate the observed trends [72]. The green synthesized CuO NPs and their integration into starch/PVA nanoscaffolds were thoroughly characterized and found to possess desirable physicochemical, thermal, morphological, and biological properties. These multifunctional composites demonstrate substantial promise for various biomedical applications, particularly in areas requiring antioxidant activity, biocompatibility, and structural versatility, such as tissue engineering, wound healing, and drug delivery.

5. CONCLUSION

The present study successfully demonstrated the green synthesis of CuO NPs using *Sargassum muticum* extract and their effective integration into starch/PVA electrospun nanoscaffolds. Comprehensive physicochemical characterizations confirmed the formation of stable, crystalline CuO NPs with notable SPR, functional group interactions, and distinct morphological features. The nanoscaffolds exhibited excellent fiber uniformity, thermal stability, and effective nanoparticle incorporation. Zeta potential and DLS analysis indicated moderate colloidal stability, while cytotoxicity assays confirmed biocompatibility with 3T3-L1 cells. Notably, the nanoscaffolds displayed enhanced antioxidant activity, surpassing the individual components, indicating a synergistic effect. These findings underscore the potential of CuO NP-incorporated biopolymer nanoscaffolds as multifunctional biomaterials for biomedical applications, especially in wound healing, drug delivery, and tissue engineering. The eco-friendly synthesis approach further supports the development of sustainable nanomaterials with significant therapeutic relevance.

Ethics declaration: Not Applicable

Conflicts of Interest: The authors declare no conflicts of interest.

Data Availability Statement: The full dataset of physiochemical characterization associated with this work is published in Mendeley Data **[Dataset]** Bioactive nanostructured platforms: Physicochemical assessment of starch scaffolds hybridized with *Sargassum muticum*-copper oxide nanoparticles (DOI: 10.17632/jrs2y2hp7v.2). Disclosure: The material characterization data and figures (e.g., UV, SEM, FTIR, XRD, TGA, Zeta Potential and particle sizer) presented here were generated from a common dataset and are being reused across multiple related studies on nanomaterials. All biological analyses and conclusions are original to each manuscript.

REFERENCES

[1] Kunamalla R, Panagal M, Palanisamy CP. Biogenic synthesis and fabrication of starch/PVA/CuO electrospun nanoscaffolds from Sargassum ilicifolium (brown marine macroalgae) extract for anticancer activity on HT-29 and MCF-7 cancer cells. Biocatalysis and Agricultural Biotechnology. 2026; 72: 103923.

[2] Pei J, Govindaraj H, Sivaramakrishnan R, Kanniappan GV, Pandurangan V, Dhayalan VK, Mironescu M, Mironescu ID, Jayaraman S, Palanisamy PC. Sustainable fabrication of biopolymer-based (starch/PVA) nanoscaffolds loaded with green-synthesized CuO nanoparticles from Sargassum wightii (marine macroalgae): Cytocompatibility and antioxidant activity. Biomaterials Advances. 2026; 182: 214660.

[3] Pei J, Perumal NC, Meng P, Long Q, Palanisamy CP. Extracellular vesicle-based biosensors for Alzheimer's disease: A new frontier in precision diagnostics. Ageing Research Reviews. 2026; 113: 102904.

[4] Shree P, Sivaramakrishnan R, Kanniappan GV, Pandurangan V, Jayaraman S, Dhayalan VK, Mironescu M, Mironescu ID, Palanisamy CP. Antioxidant and biocompatible CuO-starch/PVA nanoscaffolds via ultrasonic green synthesis using Turbinaria conoides (brown marine macroalgae). Medicine in Drug Discovery. 2025; 28: 100238.

[5] Gong J, Lin J, Guan T, Pei J, Palanisamy CP, El-AtyFrom AMA. selenium tolerance to nanoplastic antagonism: Comprehensive characterization of L. casei SNUT1 and its extracellular vesicle–nanoselenium complex. Food Bioscience. 2025; 74: 107749.

[6] Poochi SP, Sundarraj R, Raju MV, Chandrasekaran MK, Ahalliya RM, Palanisamy CP, Kanniappan GV, Kondapavuluri BK, Thiruvengadam M. Harnessing Nature: Computational and Experimental Insights Into *Ipomoea obscura* Metabolites for Bladder Cancer Therapy. Chemistry and Biodiversity. 2025; 0: e00909.

[7] Dugganaboyana GK, Kannankumar MKG, Shivaramakrishna S, Raju MV, Chandrasekaran MK, Ahalliya RM, Panneerselvam N, Palanisamy CP, Kanniappan GV. Phytochemical insights, antioxidant activity and therapeutic potential of Cassia senna against prostate cancer in Wistar albino rats. Discover Applied Sciences. 2025; 7:1206.

[8] Natarajan SR, Krishnamoorthy R, Alshuniaber MA, Gatasheh MK, Rajagopal P, Veeraraghavan VP, Palanisamy CP, Jayaraman S. KDM1A Facilitates Oncogenic Potential in Colorectal Cancer Progression Through the Activation of AXIN/GSK3β/β-Catenin Signaling Pathways: Evidence From Integrated Transcriptomics and In Vitro Studies. The Journal of Gene Medicine. 2025; 27(11): e70053.

[9] Guan T, Gong J, Lin J, Palanisamy CP, Jinjin Pei J, El-Aty AMA. Machine learning-driven multimodal optimization of selenium biotransformation and flavor profiling in fermented apple–Yacon functional beverages. Innovative Food Science & Emerging Technologies. 2025; 105: 104198.

[10] Natarajan SR, Krishnamoorthy R, Alshuniaber MA, Alsulami TS, Gatasheh MK, Rajagopal P, Palanisamy CP, Govindan R, Veeraraghavan VP, Jayaraman S. ABCE1 facilitates tumour progression via aerobic glycolysis and inhibits cell death in human colorectal cancer cells through the p53 signalling pathway. Scientific Reports. 2025; 15: 24674.

[11] Huang Y, Guo H, Liu Y, Jin W, Palanisamy CP, Pei J, Oz F, El-Aty AMA. Effects of Natural Polysaccharides on the Gut Microbiota Related to Human Metabolic Health. Molecular Nutrition & Food Research. 2025; 69:e202400792.

[12] Poornima K, Meenakshi K.C, Manikandan V.R, Shankari G, Prabhu D, Rathi M.A, Palanisamy CP, Balaji R, Gopalakrishnan V.K. Exploring the anticancer potential of Jerantinine A from *Tabernaemontana coronaria* against prostate, breast, and ovarian cancers: A computational approach. *Journal of Complementary and Integrative Medicine*, 2025 22(2): 363–372.

[13] Palanisamy CP, Poompradub S, Sansanaphongpricha K, Jayaraman S, Subramani K. Faridah Sonsudin gGreen synthesis of Nigella sativa-mediated silver nanoparticles for enhanced antibacterial activity and wound healing: Mechanistic insights and biomedical applications. Environmental Nanotechnology, Monitoring & Management. 2025; 24: 101085.

[14] Surendran N, Raju MV, Chandrasekaran MK, Ahalliya RM, Palanisamy CP, Chandrasekaran G, Kanniappan GV. Physicochemical characterization of starch from Maranta arundinacea L.(arrowroot) rhizomes and its inhibition of COX-2: In vivo validation. Bioactive Carbohydrates and Dietary Fibre. 2025; 33: 100465.
[15] Kannappan P, Chandrasekaran MK, Raju MV, Gopalakrishnan S, Dhamodharan P, Ahalliya RM, Palanisamy CP, Raju B, Kanniappan GV. Exploring the anticancer potential of Jerantinine A from Tabernaemontana coronaria against prostate, breast, and ovarian cancers: a computational approach. Journal of Complementary and Integrative Medicine. 2025; 22(02): 363-372.
[16] Pei J, Kumarasamy RV, Jayaraman S, Kanniappan GV, Long Q, Palanisamy CP. Quercetin-functionalized nanomaterials: Innovative therapeutic avenues for Alzheimer's disease management. Ageing Research Reviews. 2025; 104: 102665.
[17] Jayaraman S, Prasad M, Natarajan SR, Krishnamoorthy R, Alshuniaber MA, Gatasheh MK, Veeraraghavan VP, Rajagopal P, Palanisamy CP. Molecular mechanisms underlying the effects of beta-sitosterol on TGF-β1/Nrf2/SIRT1/p53-mediated signaling in the kidney of a high-fat diet and sucrose-induced type-2 diabetic rat. Chemico-Biological Interactions. 2025; 411: 111443.
[18] Huang Y, Guo H, Liu Y, Jin W, Palanisamy CP, Pei J, Oz F, El-Aty AMA. Effects of Natural Polysaccharides on the Gut Microbiota Related to Human Metabolic Health. Molecular Nutrition & Food Research. 2025; e202400792.
[19] Prabhakaran P, Palanisamy CP, Shanmugam A, Damodharan P, Swaminathan H, Devaraj D, Ahalliya RM, Kanniappan GV. Isolation, structural characterization, and molecular docking studies on the bioactive compound from n-Hexane extract of Emilia sonchifolia (L.) DC against the pancreatic cancer target Aurora 2 Kinase. Journal of Complementary and Integrative Medicine. 2024; 22(1): 0290.
[20] Natarajan PM, Swamikannu B, Sivaraman NM, Stylin AGSQ. Prevention of Oral Cancer: A Comprehensive Guide. Journal of Pharmacy and Bioallied Sciences. 2024; 16(5): S4239-S4241.
[21] Umapathy V, Dhanavel A, Kesavan R, Natarajan PM, Bhuminathan S, Vijayalakshmi P. Anticancer Potential of the Principal Constituent of Piper nigrum, Piperine: A Comprehensive Review. Cureus. 2024; 16(2): e54425.
[22] Umapathy VR, Swamikannu B, Natarajan PM, Devi R, Nandini MS, Vimalarani, Vijayalakshmi P. In Silico Molecular Docking of Ocimum sanctum Phytochemicals: Targeting Key Biomarkers in Oral Cancer. Journal of Pharmacy and Bioallied Sciences. 2024; 16(5): S4792-S4799.
[23] Natarajan PM, Bhuminathan S, Rajan R, Bindu K, Loganathan K, Veerakumar R. The Crucial Role of Smoking Cessation in Preventing Oral Cancer. Journal of Pharmacy and Bioallied Sciences. 2024; 16(5): S4245-S4247.
[24] Swamikannu B, Umapathy VR, Natarajan PM, Nandini MS, Stylin AGSQ, Vimalarani V, Rajinikanth S. Unlocking the Therapeutic Benefits of Artemisia Annua: A Comprehensive Overview of its Medicinal Properties. Journal of Pharmacy and Bioallied Sciences. 2024; 16(5): S4248-S4253.
[25] Natarajan PM. Computational Studies on Recent Congeners of Fluoroquinolones and Nitroimidazoles for Their Use in Periodontal Therapy. Journal of Pharmacy and Bioallied Sciences. 2024; 16(5): S4731-S4740.
[26] Yadalam PK, Arumuganainar D, Natarajan PM, Ardila CM. Artificial intelligence-powered prediction of AIM-2 inflammasome sequences using transformers and graph attention networks in periodontal inflammation. Scientific Reports. 2025; 15: 8733.
[27] Yadalam PK, Chatterjee S, Natarajan PM, Ardila CM. Comparison of light gradient boosting and logistic r egression for interactomic hub genes in Porphyromonas gingivalis and Fusobacterium nucleatum-induced periodontitis with Alzheimer's disease. Frontiers in Oral Health. 2025; 6:1463458.
[28] Jiang H, Kumarasamy RV, Pei J, Raju K, Kanniappan GV, Palanisamy CP. Integrating engineered nanomaterials with extracellular vesicles: Advancing targeted drug delivery and biomedical applications. Frontiers in Nanotechnology. 2024; 6: 1513683.
[29] Guo H, Liu Y, Wan T, Song D, Palanisamy CP, Geng J, Pei J, Özmen S, El-Aty AMA. Toward personalized cancer management: Role of precision nutrition–diet interventions. Journal of Functional Foods. 2024; 123: 106584.
[30] Natarajan SR, Krishnamoorthy R, Alshuniaber MA, Al-Anazi KM, Farah MA, Rajagopal P, Palanisamy CP, Veeraraghavan VP, Jayaraman S. Identification of FOXM1 as a novel protein biomarker and therapeutic target for colorectal cancer progression: Evidence from immune infiltration and bioinformatic analyses. International Journal of Biological Macromolecules. 282 (Part 4): 137201.
[31] Rajendran MS, Jayaraman S, Khan JM, Jasmine S, Prabhakaran RK, Raju MV, Chandrasekaran MK, Ahalliya RM, Kannappan P, Palanisamy CP, Kanniappan GV. Investigating the colon toxicity and carcinogenic role of monosodium glutamate compared with Dimethylhydrazine in male Wistar rats: Exploring the link to childhood colon cancer risk. Journal of King Saud University - Science. 2024; 36(11): 103507.
[32] Kumarasamy RV, Natarajan P, Umapathy VR, Roy JR, Rab SO, Saeed M, Panagal M, Mironescu M, Srinivasan GP, Palanisamy CP. Clinical Applications and Therapeutic Potentials of Advanced Nanoparticles: A Comprehensive Review on Completed Human Clinical Trials. Frontiers in Nanotechnology. 2024; 6:1479993.

[33] Jin W, Pei JJ, Roy JR, Jayaraman S, Ahalliya RM, Kanniappan GV, Mironescu M, Palanisamy CP. Comprehensive review on single-cell RNA sequencing: A new frontier in Alzheimer's disease research. Ageing Research Reviews. 2024; 274: 102454.
[34] Pei J, Palanisamy CP, Jayaraman S, Natarajan PM, Umapathy VR, Roy JR, Panagal M, Jayaraman S. Curcumin-loaded polymeric nanomaterials as a novel therapeutic strategy for Alzheimer's disease: A comprehensive review. Ageing Research Reviews. 2024; 99: 102393.
[35] Pei J, Palanisamy CP, Jayaraman S, Natarajan PM, Umapathy VR, Roy JR, Thalamati D, Ahalliya RM, Kanniappan GV, Mironescu M. A comprehensive review on starch-based Sustainable Edible Films Loaded with Bioactive Components for Food Packaging. International Journal of Biological macromolecules. 2024; 274 (Part-1): 133332.
[36] Palanisamy CP, poompradub S, Sansanaphongpricha K, Subramani K, Sonsudin F. Increased expression levels of PDGF and VEGF magnify the wound healing potential facilitated by biogenic synthesis of silver nanoparticles. Nano-Structures & Nano-Objects. 2024; 39: 101236.
[37] Pei J, Palanisamy CP, Jayaraman S, Natarajan PM, Umapathy VR, Roy JR, Thalamati D, Ahalliya RM, Kanniappan GV, Mironescu M. Proteomics Profiling of Extracellular Vesicle for Identification of Potential Biomarkers in Alzheimer's Disease: A Comprehensive Review. Ageing Research Reviews. 2024; 99: 102359.
[38] Xi J, Wang T, Xian P, Liu X, Du M, Yang H, Palanisamy CP, Lin W, Long Q. Proteomic insights uncover enhanced neurotherapeutic potential in conditioned mesenchymal stem cell-derived extracellular vesicles. Extracellular Vesicle. 2024; 3: 100037.
[39] Pei J, Natarajan PM, Umapathy VR, Swamikannu B, Sivaraman NM, Krishnasamy L, Palanisamy CP. Advancements in the synthesis and functionalization of zinc oxide-based nanomaterials for enhanced oral cancer therapy. Molecules. 2024; 29(11): 2706.
[40] Gatasheh MK, Natarajan SR, Krishnamoorthy R, Alsulami TS, Rajagopal P, Palanisamy CP, Veeraraghavan VP, Jayaraman S. Molecular analysis to identify novel potential biomarkers as drug targets in colorectal cancer therapy: an integrated bioinformatics analysis. Molecular and Cellular Oncology. 2024; 11(1): 2326699.
[41] Pei J, Yan Y, Jayaraman S, Rajagopal P, Natarajan PM, Umapathy VR, Gopathy S, Roy JR, Sadagopan CS, Thalamati D, Palanisamy CP, Mironescu M. A review on advancements in the application of starch-based nanomaterials in biomedicine: Precision drug delivery and cancer therapy. International Journal of Biological Macromolecules. 2024; 130746.
[42] Pei JJ, Yan Y, Palanisamy CP, Jayaraman S, Natarajan PM, Umapathy VR, Gopathy S, Roy JR, Sadagopan JC, Thalamati D, Mironescu M. Materials-based drug delivery approaches: Recent advances and future perspectives. Green Processing and Synthesis. 2024; 13: 20230094.
[43] Pei JJ, Deng W, Liu Y, Guo Y, Chen J, Abdu H, Khan MR, Palanisamy CP, El-Aty AM. A Comprehensive Review of Cornus officinalis: Health Benefits, Phytochemistry, and Pharmacological Effects for Functional Drug and Food Development. Frontiers in Nutrition. 2023; 10: 1309963.
[44] Alugoju P, Palanisamy CP, Anthikapalli NVA, Jayaraman S, Prasanskulab A, Chuchawankul S, Dyavaiah M, Tencomnao T. Exploring the anti-aging potential of natural products and plant extracts in budding yeast Saccharomyces cerevisiae: A review. F1000Research. 2023; 12: 1265.
[45] Lavanya M, Krishnamoorthy R, Alshuniaber MA, Manoharadas S, Palanisamy CP, Veeraraghavan VP, Jayaraman S, Rajagopal P, Padmini R. Formulation, characterization and evaluation of gelatin-syringic acid/zinc oxide nanocomposite for its effective anticancer, antioxidant and anti-inflammatory activities. Journal of King Saud University-Science. 2023; 35: 102909.
[46] Palanisamy CP, Poompradub S, Sansanaphongpricha K, Jayaraman S, Subramani K, Sonsudin F. Biosynthesis of silver nanoparticles (AgNPs) using ethanolic extract of Nigella sativa (L.) seeds promotes wound healing via PDGF and VEGF signalling pathways activation. Biocatalysis and Agricultural Biotechnology. 2023; 54: 102970.
[47] Prasad M, Jayaraman S, Natarajan SR, Veeraraghavan VP, Krishnamoorthy R, Gatasheh MK, Palanisamy CP, Elrobh M. Piperine modulates IR/Akt/GLUT4 pathways to mitigate insulin resistance: Evidence from animal and computational studies. International Journal of Biological Macromolecules. 2023; 253: 127242.
[48] Palanisamy CP, Pei JJ, Phaniendra A, Venkata AAN, Jayaraman S, Veeraragahavan VP, Sridevi G, Roy JR, Janaki CS, Thalamati D, Mironescu M, Luo Q, Chai Y, Long Q. New Strategy of Neurodegenerative Disease Treatment with Extracellular Vesicles (EVs) Derived from Mesenchymal Stem Cells (MSCs). *Theranostics*. 2023; 13(12):4138-4165. doi:10.7150/thno.83066.
[49] Natarajan PM, Umapathy VR, Murali A, Swamikannu B. (2022). Computational Simulations of Identified marine-derived Natural Bioactive Compounds As Potential Inhibitors of Oral Cancer. Future Science OA. 2022; 8(3).
[50] Natarajan PM, Umapathy VR. Role of transcriptomics in the study of oral cancer. Frontiers in Oral Health. 2025; 6:1524364.
[51] Vidhyarekha U, Natarajan PM, Bhuminathan S, Sabarinathan J, Suba R, Vijayalakshmi P. Role of artificial intelligence in Oral Cancer. Advances in Public Health. 2024. 2024: 3664408.

[52] Ganesan A, Kumar NG, Natarajan PM, Gauthaman J. Automated classification of elongated styloid processes using deep learning models-an artificial intelligence diagnostics. Frontiers in Oral Health. 2025; 5: 1424840.
[53] Umapathy VR, Natarajan PM, Swamikannu B. Regenerative Strategies in Dentistry: Harnessing Stem Cells, Biomaterials and Bioactive Materials for Tissue Repair. Biomolecules. 2025; 15: 546.
[54] Natarajan PM. Dental Bioinformnatics-Current Scope and Future perspectives. Research Journal of Pharmacy and Technology. 2022;15(5):2351-6.
[55] Ganesan A, Kumar NG, Natarajan PM. Solanum trilobatum leaf extract-derived silver nanoparticles downregulate the PI3K/AKT/mTOR signaling pathway and attenuate oral squamous cell carcinoma cell proliferation. Journal of Herbmed Pharmacology. 2024; 13(2): 300-307.
[56] Perumal MKK, Renuka RR, Subbiah SK, Natarajan PM. Artificial intelligence-driven clinical decision support systems for early detection and precision therapy in oral cancer: a mini review. Frontiers in Oral Health. 2025; 6: 1592428.
[57] Ramesh E, Ganesan A, Lakshmi KC, Natarajan PM. Artificial intelligence-based diagnosis of oral leukoplakia using deep convolutional neural networks Xception and MobileNet-v2. Frontiers in Oral Health. 2025; 6: 1414524.
[58] Ganesan A, Kumar NG, Natarajan PM. Anticancer activity of silver nanoparticles synthesized from aqueous leaf extract of Solanum trilobatum (Purple fruit pea eggplant) on human oral cancer cells. Journal of Herbmed Pharmacololgy. 2024; 13(2): 260-268.
[59] Daniel Raja FS, Abraham L, Rangasamy K, Saikia K, Rathankumar AK, Mironescu M, Mironescu I, Palanisamy CP, Kanniappan GV. Next-Generation Microbiome Therapeutics: Psychobiotics and Fecal Microbiota Transplants (FMT) for Mental Health Treatment. Frontiers in Cellular and Infection Microbiology. 2026; 16: 1719357.
[60] Dharmaprakash S, Gunasekaran VP, Sivaramakrishnan R, Kanniappan GV, Jayaraman S, Mironescu M, Rajabathar JR, Mironescu ID, Palanisamy CP. Marine macroalgae-mediated ultrasonic-assisted green synthesis of CuO nanoparticles embedded in starch/PVA electrospun nanoscaffolds for in vitro α-amylase and α-glucosidase inhibitory activity. Scientific Reports. 2026.
[61] Surendran N, Chandrasekaran G, Raju MV, Chandrasekaran MK, Ahalliya RM, Palanisamy CP, Kanniappan GV, Arcot R, Alharbi NS, Thiruvengadam M. Anti-inflammatory potential of ethanolic extract of Maranta arundinacea L.: Insights from COX-2 modulation and oxidative stress analysis. South African Journal of Botany. 2026; 195: 142-151.
[62] Pei J, Senthilkumar MV, Hessini K, Subramaniyam S, Sivaramakrishnan R, Kanniappan GV, Jayaraman S, Palanisamy CP. Green fabrication of starch/PVA/CuO nanoscaffolds using marine macroalgae extract for enhanced anti-inflammatory activity. Sustainable Chemistry and Pharmacy. 2026; 51: 102397.
[63] Balasubramanian V, Loganathan L, Muthuswamy K, Viswanathan TM, Raju MV, Chandrasekaran MK, Ahalliya RM, Poorasamy J, Palanisamy CP, Dominic S, Kanniappan GV. Anticancer therapeutic efficacy of PEGylated β-galactosidase from Aspergillus terreus in DMBA-induced breast cancer: Toxicological, molecular and histopathological evaluation in Wistar rats. International Journal of Biological Macromolecules. 2026; 360: 151856.
[64] Jayaraman S, Eswaran A, Rajagopal P, Palanisamy CP, Veerakumar P, Veeraraghavan VP, Sirasanagandla SR. Neuroendocrine-associated epigenetic factors in cellular senescence: mechanisms and therapeutic implications. Biogerontology. 2026; 27(2): 64.
[65] Ponnusamy B, Rajagopal P, Palanisamy CP, Veeraraghavan VP, Jayaraman S. Mechanistic Exploration of the anticancer activity of Justicia adhatoda Plant Leaf Ethanolic Extract against Colon Cancer Cells: An in silico and in vitro Approach. Asian Pacific Journal of Cancer Prevention. 2026; 27(3): 1069-1080.
[66] Pei J, Saran VS, Sivaramakrishnan R, Kanniappan GV, Pandurangan V, Jayaraman S, Dhayalan VK, Mironescu M, Mironescu ID, Palanisamy CP. Ultrasonic-assisted, Sargassum ilicifolium (brown marine macroalgae)-mediated biogenic synthesis of CuO nanoparticles incorporated in starch/PVA electrospun nanoscaffolds: In vitro safety and antioxidant efficacy assessment. Bioorganic Chemistry. 2026; 173: 109679.
[67] Raj MAPA, Subramaniyam S, Kanniappan GV, Jayaraman S, Palanisamy CP. Sustainable fabrication of starch/PVA/CuO electrospun nanoscaffolds from Turbinaria ornata (marine macroalgae) extract: Physicochemical characterization and antidiabetic evaluation. Kuwait Journal of Science. 2026; 53(2): 100545.
[68] Pei J, Ganesh NS, Subramaniyam S, Sivaramakrishnan R, Kanniappan GV, Jayaraman S, Palanisamy CP. Sustainable fabrication of starch/PVA/CuO electrospun nanoscaffolds from Padina tetrastromatica (Brown macroalgae) extract: Physicochemical characterization and antidiabetic assessment. Sustainable Chemistry One World. 2026; 9: 100195.
[69] Sakthiraj A, Sivaramakrishnan R, Subramaniyam S, Kanniappan GV, Pandurangan V, Jayaraman S, Dhayalan VK, Mironescu M, Mironescu ID, Palanisamy CP. Starch/PVA electrospun nanoscaffolds loaded with ultrasonic-assisted green-synthesis of CuO nanoparticles from marine macroalgae (Gracilaria corticata) extract: Cytotoxicity and antioxidant analysis. Chemical Physics Impact. 2026; 12: 101018.

[70] Raju M, Chandrasekaran MK, Loganathan L, Ahalliya RM, Mironescu M, Mironescu ID, Palanisamy CP, Kanniappan GV. Lipid remodeling and ferroptosis in phosphatidylcholine-mediated tumor–stroma crosstalk. Frontiers in Molecular Biosciences. 2026; 13: 1742305.
[71] Natarajan PM, Bhuminathan S, Leela B, Bindu K, Loganathan K, Ramachandran V. Smoking and its Role in Oral Cancer. Journal of Pharmacy and Bioallied Sciences 16(5): S4242-S4244.
[72] Yadalam PK, Natarajan PM, Ardila CM. Variational graph autoencoder for reconstructed transcriptomic data associated with NLRP3 mediated pyroptosis in periodontitis. Scientific Reports. 2025; 15: 1962.